Electron paramagnetic resonance of photochromic Fe^{2+}-O^{-} in $SrTIO_3$

1993 J. Phys.: Condens. Matter 5 361

(http://iopscience.iop.org/0953-8984/5/3/011)

J. Phys.: Condens. Matter 5 (1993) 361–370. Printed in the UK

Electron paramagnetic resonance of photochromic Fe^{2+}–O^- in $SrTiO_3$

Th W Kool and M Glasbeek

Laboratory for Physical Chemistry, University of Amsterdam, Nieuwe Achtergracht 127, 1018 WS Amsterdam, The Netherlands

Received 17 August 1992

Abstract. A new photochromic hole centre in $SrTiO_3$, trapped at an oxygen anion site near an iron impurity and thermally stable below 35 K, is reported. The hole is characterized by $S = \frac{1}{2}$ and has been studied by means of EPR. The hole is of orthorhombic local symmetry and its spin-Hamiltonian parameters are given as: $g_1 = 2.0071 \pm 0.0005$, $g_2 = 2.0180 \pm 0.0005$ and $g_3 = 2.0515 \pm 0.0005$, the magnetic main axes being along the [110], [$1\bar{1}0$] and [001] crystallographic directions. Hyperfine interaction with a nuclear spin of $I = \frac{1}{2}$ in a 2.21% natural abundance was also resolved. The hyperfine splittings are given by $|A_1| = 19.6 \pm 0.5$ MHz, $|A_2| = 16.9 \pm 0.5$ MHz and $|A_3| = 11.5 \pm 0.5$ MHz. The hole is identified as the Fe^{2+}–O^- centre. Under the influence of applied static electric fields the hole centre main axes undergo a reorientation. From the measurements, an electric dipole moment of $\mu = 5.07 \times 10^{-4}$ e Å at 20 K was determined. Upon the application of uniaxial stress the hole centre main axes are also reoriented. From the measurements at 30 K, a differential stress coupling coefficient of $\beta_{[001]} = 3.48 \times 10^{-24}$ cm^3 could be determined.

1. Introduction

Previously, EPR investigations in $SrTiO_3$ have shown the presence of hole centres of tetragonal symmetry trapped at O^{2-} sites near Ti^{4+} [1] and substitutional V^{5+} [2]. Holes of orthorhombic symmetry and trapped at O^{2-} ions neighbouring Mg^{2+} and Al^{3+} impurities have also been found in $SrTiO_3$ [3]. Here we report on an EPR investigation of a new hole centre, of orthorhombic local symmetry, in $SrTiO_3$. The characteristics of this hole centre have been studied under the influence of applied electric fields and uniaxial stresses. The experiments show that under the influence of these external fields the magnetic axes of the hole centre undergo a reorientation. This can be concluded from changes in the relative intensities of the EPR lines, representative of the six magnetically inequivalent hole centre sites, upon the application of the external fields. The intensity effects are analogous to those previously found elsewhere in EPR studies of the O_2^- molecular ion in alkali halides [4].

2. Experimental details

Single crystals of $SrTiO_3$ containing vanadium (60 ppm) and iron (16 ppm) were purchased from Semi-Elements Inc. EPR measurements were made by means of a

0953-8984/93/030361+10$07.50

Varian E-6 spectrometer operating at X-band (9.33 GHz). The signals were obtained utilizing 100 kHz modulation. The sample was mounted in an optical transmission cavity. Hole centre EPR spectra could be recorded at temperatures between 1.8 K and 35 K. For the EPR measurements at liquid helium temperatures, a stainless steel cryostat with a quartz tip was used. For higher temperatures, a variable temperature accessory was used. The hole centre discussed below was obtained after illumination of the sample with light from a Philips SP 500 W high-pressure mercury arc lamp in line with a 396 nm interference filter of 0.9 nm bandwidth.

Uniaxial stress experiments were performed with the help of a device, which transforms the hydrostatic pressure in a gas chamber through a connection with a stainless steel rod into a uniaxial stress exerted on the crystal [5]. Uniaxial stresses were applied perpendicular to the magnetic field direction. Stresses up to 10×10^8 dyne cm^{-2} were achieved.

Static electric fields were applied across the crystal by connecting a DC high voltage power supply with copper electrodes, which were mounted to gold electrode coatings on the crystal. Static electric fields up to 13 kV cm^{-1} were applied.

3. Results

After continuous illumination of the $SrTiO_3$ crystal with light at a wavelength of 396 nm, we observed at 30 K, in addition to the EPR spectrum of the V^{4+} impurity ion [5, 6], four new EPR lines. In figure 1(*a*), part of the total EPR spectrum is displayed, showing the magnetic field region where the four new resonance lines are observed, as indicated by the arrows, for a magnetic field H oriented in an (001) plane and about 40° from the [010] crystallographic axis. In figure 2, the angular dependence of the EPR lines is shown when the magnetic field is rotated in the (001) plane of the crystal. The experimental data (as indicated by points) show a good fit with the computer simulations (as indicated by the full curves) for an $S = \frac{1}{2}$ centre of orthorhombic local symmetry, for the g values given in table 1, column 2. The orientation of the main axes of the six orthorhombic sites are as labelled in figure 3. The intensity ratios of the EPR lines are as indicated by the numbers in parentheses in figure 2.

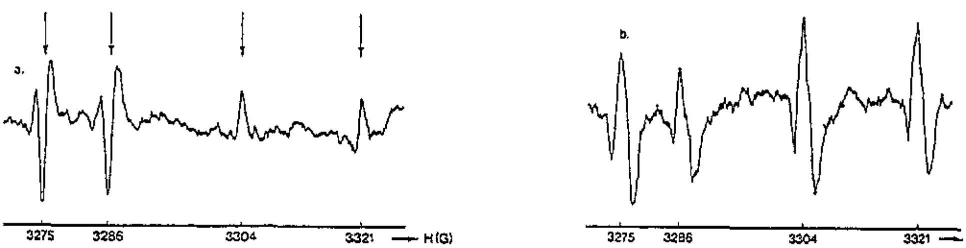

Figure 1. (*a*) The EPR spectrum of the Fe^{2+}–O^- hole centre in $SrTiO_3$ after illumination of the crystal with 396 nm light. H is oriented in the (001) plane and about 40° from the [010] axis, $T = 30$ K. (*b*) The influence of [001] stress on the intensities of the EPR lines of Fe^{2+}–O^- at $T = 30$ K; $\sigma_{[001]} = 2.37 \times 10^8$ dynes cm^{-2}.

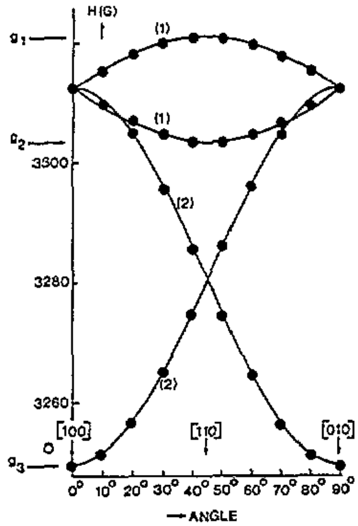

Figure 2. The angular dependence of the EPR lines of Fe^{2+}–O^- in $SrTiO_3$ with $\boldsymbol{H}$ rotated in the (001) plane. The points represent the experimental data. The numbers in parentheses represent the relative intensities of the lines.

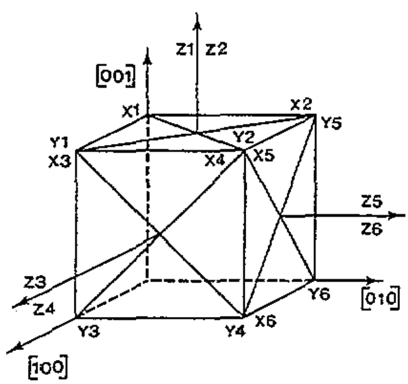

Figure 3. Labelling of the Fe^{2+}–O^- hole centres and the directions of the principal centre axes. $x = g_1$, $y = g_2$ and $z = g_3$.

The signal-to-noise ratio of the EPR lines improved considerably when an electric field was applied. As a result, hyperfine interaction with an $I = \frac{1}{2}$ nuclear spin in only a 2.21% abundance could now also be observed. An illustrative example is given in figure 4. With a spin Hamiltonian of the form

$$\mathcal{H} = \mu_B \boldsymbol{H} \cdot \mathbf{g} \cdot \boldsymbol{S} + \boldsymbol{S} \cdot \mathbf{A} \cdot \boldsymbol{I} \tag{1}$$

the $\mathbf{g}$- and $\mathbf{A}$-tensor elements giving the best fit values to the experimental data are summarized in column 2 of table 1. No additional splittings due to the 105 K structural phase transition [7, 8] could be resolved. When the temperature was increased, the intensities of the hole centre EPR lines decreased until above 35 K

Table 1. g and A values for orthorhombic O^- p(π) hole centres in $SrTiO_3$.

	Fe^{2+}–O^-	Al^{3+}–O^-	Mg^{2+}–O^-
g_1	2.0071	2.0100	2.0098
g_2	2.0180	2.0175	2.0233
g_3	2.0515	2.0515	2.0477
$\|A_1\|$ (MHz)	19.6±0.5	16.3±0.3	—
$\|A_2\|$ (MHz)	16.9±0.5	16.1±0.3	—
$\|A_3\|$ (MHz)	11.5±0.5	14.3±0.3	—
a (MHz)	−16.0±0.5	−15.6±0.3	—
b (MHz)	2.25±0.5	0.6±0.3	—
e (MHz)	1.35±0.5		

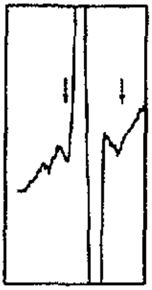

Figure 4. Hyperfine structure as observed for the EPR line at H = 3318 G of the Fe^{2+}–O^- centre, due to the ^{57}Fe ($I = \frac{1}{2}$) isotope.

the spectrum could no longer be observed. Concomitantly, the EPR spectrum due to the I_1 centre [9] appeared above 35 K. At temperatures higher than 50 K, the latter spectrum also disappeared and the EPR spectrum of the Fe^{5+} impurity centre is observed [10]. These observations are analogous to those reported in [3].

Upon the application of uniaxial stress along the pseudo-cubic [001] axis, with the magnetic field $\boldsymbol{H}$ in the (001) plane and perpendicular to the stress, the following changes in the EPR spectrum are observed. The intensities of the EPR signals due to sites 1 and 2 are enhanced relative to the intensities of the EPR signals associated with sites numbered 3,4 and 5,6. The effect is illustrated in figure 1. When a stress of 2.37×10^8 dynes cm^{-2} along the [001] direction is applied, the spectrum of figure 1(a) is changed into the spectrum of figure 1(b). Clearly, in this case the relative intensities of the resonances at 3304 G and 3321 G (due to sites 1 and 2) are enhanced. No line shifts were observed.

Upon the application of a static electric field $\boldsymbol{E}$ along the pseudo-cubic [010] axis, with the magnetic field $\boldsymbol{H}$ in the (001) plane, the following changes in the EPR spectrum are observed. The intensities of the EPR lines due to sites 1 and 2, and 3,4 are enhanced in intensity relative to the intensities of the EPR lines associated with sites 5 and 6. The effect is illustrated in figure 5. When an electric field of 10.5 kV cm^{-1} at 20 K is applied, the spectrum of figure 5(a) is changed into the spectrum of figure 5(b). In this case the relative intensity of the resonance at 3257 G (due to sites 5 and 6) is lowered. Again, no line shifts were observed.

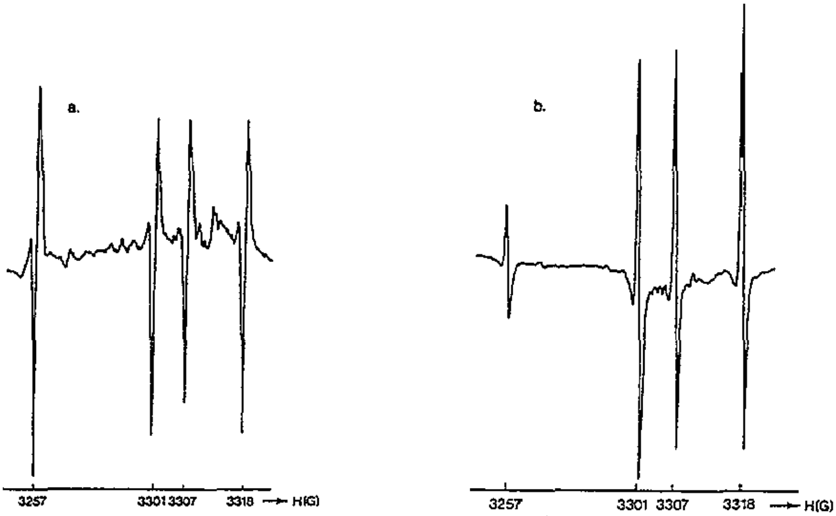

Figure 5. (*a*) The EPR spectrum of the Fe^{2+}–O^- centre for H oriented in the (001) plane and about 20° from the crystallographic [100] axis, T = 20 K. (*b*) The same spectrum, but now for the crystal in an electric field $E \| [010]$, E = 10.5 kV cm^{-1}.

4. Discussion

4.1. Characterization of the centre

For an arbitrary orientation of the magnetic field in the (001) plane, the observed orthorhombic EPR spectrum consists of four lines with an intensity ratio of 1:1:2:2 (cf figure 2). Our assignment that the new lines are due to a hole centre is largely based on the positive g shifts. Furthermore, the g values show a large similarity to those found previously for the Al^{3+}–O^- and Mg^{2+}–O^- [3] hole centres in $SrTiO_3$ (cf table 1). We tentatively assign the paramagnetic entity to a hole trapped at an oxygen site. However, the O^- hole centre reported here differs from the Al^{3+}–O^- and the Mg^{2+}–O^- hole centres in $SrTiO_3$ as regards the orientation of the magnetic main axes in the crystal, namely [110], [1$\bar{1}$0] and [001] versus [100], [010] and [001], respectively. For the Al^{3+}–O^- and Mg^{2+}–O^- centres, a hole trapped in the p(π) orbital, the latter being perpendicular to the Al^{3+}–O^- or Mg^{2+}–O^- bond direction, was assumed. To explain the fact that the magnetic main axes are along the {100} directions, it was proposed [3] that the hole is not localized in either of the two possible equivalent p(π) orbitals (pointing to the [110] and [1$\bar{1}$0] directions) but rather is involved in a rapid hopping process; for the hole centre reported here such a hopping need not be invoked.

The acceptor defect causing the trapping of the hole most likely is diamagnetic ($S = 0$), since the $S = \frac{1}{2}$ hole centre does not exhibit magnetic interactions with other electron spins. The two small hyperfine lines around each main EPR line (figure 4) are attributed to a hyperfine interaction with ^{57}Fe ($I = \frac{1}{2}$, natural abundance 2.21%). Iron is nearly always present in $SrTiO_3$, even in nominally 'pure' crystals. Due to the large dielectric constant of $SrTiO_3$, iron can be present in a large variety of valence states ranging from 1+ to 5+ [11–13]. In particular, Fe^{2+} is likely to trap the light-induced hole centre observed here for a number of reasons. Firstly, one expects that Fe^{2+}, if present, is diamagnetic ($S = 0$). Secondly, Fe^{2+} will be substitutional for

Ti^{4+}, since the ionic radius of Fe^{2+} is 0.61 Å [14], which is almost equal to that of Ti^{4+} (with an ionic radius of 0.64 Å [14]). Finally, Fe^{2+} due to its negative charge with respect to the Ti^{4+} ion that it replaces could readily act as a trap for the positively charged hole. The p orbital which accommodates the hole is then stabilized by one of the d_{xy}, d_{yz} or d_{xz} orbitals of the ground state of the Fe^{2+} ion (cf figure 6). In a LCAO-MO description of the Fe^{2+}–O^- hole centre, the hole is trapped in a MO which is a linear combination of a $p(\pi)$ orbital originating from O^- and one of the t_{2g} orbitals of the Fe^{2+} ion. The result is six inequivalent sites in the crystal, as indeed observed in the EPR experiment.

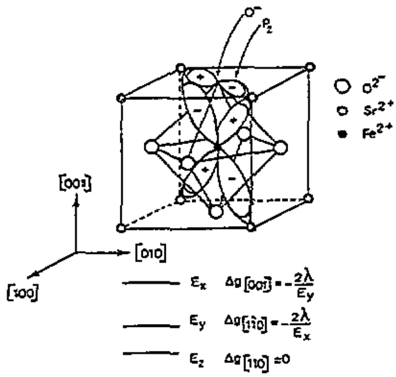

Figure 6. A model of the hole trapped at an O^{2-} ion, the Fe^{2+} ion being at the centre of the $SrTiO_3$ unit cell.

The proposed model is also supported by comparison of the isotropic Fermi contact interaction a of the orthorhombic Fe^{2+}–O^- hole centre with that of the Al^{3+}–O^- hole centre in $SrTiO_3$ (cf table 1, columns 1 and 2). With the help of the following expressions [15]:

$$A_3 = a + 2b \qquad A_2 = a - b - e \qquad A_1 = a - b + e \tag{2}$$

we calculated the isotropic Fermi contact interaction a, the axial dipolar interaction b and the orthorhombic dipolar interaction e (see table 1, column 1). Because $|A_3| < |A_2|, |A_1|$, a has to be negative. The magnitude and negative sign of a is consistent with the model of a diamagnetic Fe^{2+} ion lying near a nodal plane of the p_z orbital, causing superhyperfine interaction by exchange polarization of the diamagnetic Fe^{2+} ion closed shells [16, 17]. A hole centre with similar g values ($g_1 = 2.010$, $g_2 = 2.020$ and $g_3 = 2.070$) and similar orientations for the principal axes has been found in $BaTiO_3$ [18]. However, in the latter case the acceptor defect causing the trapping of the hole has not been identified.

4.2. Electric field and stress effects

As detailed in section 3, upon the application of a static electric field along the [010] crystallographic direction, changes in the relative intensities of the EPR lines stemming from the six magnetically inequivalent hole centre sites are observed. The results are readily understood assuming a six-fold orientational degeneracy of the electric dipole associated with each hole centre in zero field. Under the influence of the applied electric field the degeneracy is partially lifted into a four-fold degenerate lower level and a two-fold degenerate higher level. Due to thermal equilibrium the lower level is preferentially populated, resulting in differences in the intensities of the EPR lines corresponding to the inequivalent sites. The EPR lines due to the hole centres numbered 1, 2, 3 and 4 are enhanced relative to those of sites 5 and 6 (cf figure 5). The reorientation effect is in favour of those sites with a component of their $p_z(\pi)$ orbital along the electric field. This behaviour is comparable to the reorientation behaviour of $[Li]^0$ and V^- hole centres in CaO [19].

The electric dipole moment, μ, associated with the hole centre was determined by plotting I_E/I versus E_{loc}, where I_E is the integrated line intensity due to sites numbered 3 and 4, and I is the integrated line intensity due to sites numbered 5 and 6 (cf figure 7). The local electric field, E_{loc}, 'seen' by the hole centre differs from the macroscopic applied electric field and, in general, is larger than the applied electric field [20, 21]. For $SrTiO_3$, which is highly polarizable at low temperatures, the internal local field is expressed in terms of the polarization as $E_{loc} = P/\epsilon_0$. The polarization as a function of the external field at 20 K was obtained from [22]. In accordance with Boltzmann's population distribution law, we find experimentally that the EPR line intensities change as

$$I_E/I = \cosh(\mu E_{loc} \cos\theta/kT) \tag{3}$$

where θ represents the angle between the hole centre dipole moment and the local electric field directions. The drawn curve in figure 7 displays the best fit result for the functional behaviour given by equation (3). We thus find $\mu = 8.13 \times 10^{-32}$ C m = $5.07 \times 10^{-4} e$ Å, which is smaller than the values found for the $[Li]^0$ and V^- centres in MgO and CaO [19].

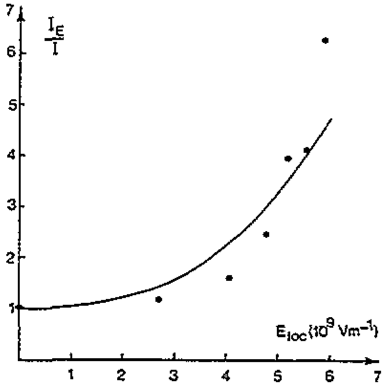

Figure 7. A plot of the intensity ratio I_E/I versus E_{loc}, where I_E is the integrated line intensity due to sites numbered 3 and 4, and I is the integrated line intensity due to sites numbered 5 and 6, $E \| [010]$. The ratio was normalized to unity for $E = 0$. The full curve is a least-square fit to a coth function.

We now turn to the reorientation effects under the influence of uniaxial stress. When uniaxial stress is applied along the [001] crystallographic direction,

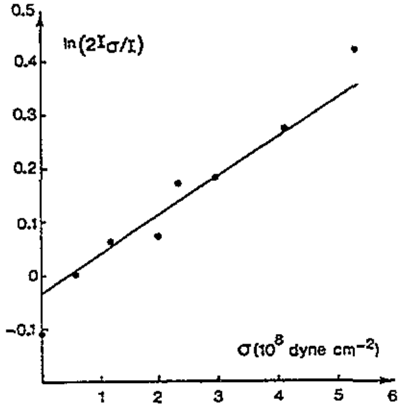

Figure 8. A plot of the intensity ratio $\ln(2I_\sigma/I)$ versus the external stress σ ($\sigma \| [001]$) for the Fe^{2+}–O^-:$SrTiO_3$ system. The full line is a least-square fit to a straight line.

the reorientation is in favour of sites 1 and 2, which have their $p_z(\pi)$ orbitals perpendicular to the stress direction. This stress behaviour is analogous to that of the $[Li]^0$ and V^- hole centres in CaO [19]. The uniaxial stress apparently lifts a six-fold orientational degeneracy into a two-fold degenerate lower energy level and a four-fold degenerate higher energy level. Thermal equilibrium maintains the preferential population of the lower levels and hence one will find differences in the intensities of the EPR lines corresponding to the different sites. In figure 8 the behaviour of $\ln(2I_\sigma/I)$ is plotted as a function of the [001] uniaxial stress magnitude. A deviation of the semi-logarithmic behaviour representative of non-linear behaviour effects is found for stresses higher than 6×10^8 dyne cm^{-2}.

In analysing the experimental data we make use of the idea of an 'elastic' dipole [23]. In the classical continuum theory the energy of the elastic dipole is given as [24]

$$U = -\frac{1}{2}\sigma \cdot e = -\frac{1}{2}\sum_{i,j} \sigma_{ij} e_{ij} \tag{4}$$

where σ is the stress tensor, e the strain tensor and i, j run over the Cartesian components x, y and z. For a low concentration of defects the strain can be expressed in powers of the defect concentration:

$$e_{ij}(n) = e_{ij}(0) + n(\partial e_{ij}/\partial n)_{n=0} + \dots \tag{5}$$

where n is the number of defects per unit volume. The (dimensionless) elastic dipole tensor is defined by

$$\lambda_{ij} = (1/V_0)(\partial e_{ij}/\partial n)_{n=0}. \tag{6}$$

From equations (4)–(6) we obtain

$$\Delta U = -V_0 \boldsymbol{\lambda} \cdot \sigma \equiv \beta \cdot \sigma \tag{7}$$

where β is the linear stress coupling tensor, with the dimension of a volume. The $\boldsymbol{\lambda}$ tensor can be divided into an isotropic part and an anisotropic part, λ', where λ'

has zero trace [25]. For uniaxial stress along [001], the differential stress coupling coefficient $\beta_{[001]}$ of an orthorhombic defect in a solid of cubic symmetry is given as [23]

$$\beta_{[001]} = V_0[\tfrac{1}{2}(\lambda_1' + \lambda_2') - \lambda_3'] \tag{8}$$

where λ_1', λ_2' and λ_3' are the principal values of the λ' tensor. Under Boltzmann equilibrium conditions, the intensity ratio of the EPR lines due to the elastic dipole is

$$2I_\sigma/I = \exp(\beta_{[001]}\sigma/kT) \tag{9}$$

where I_σ is the integrated intensity of the EPR lines due to centres 1 (or 2) and I is the integrated line intensity due to centres numbered 3 and 4 (or 5 and 6). In figure 8 we plot the experimental values as a function of σ. From the slope of the least-square fit line we find $\beta = 3.48 \times 10^{-24}$ cm^3. This value is of the order of the values found for the V^- centres in MgO and CaO [19].

5. Conclusion

In conclusion we report the observation of a new photochromic hole trapped on an O^{2-} p(π) orbital next to an Fe^{2+} ion substitutional for Ti^{4+} in $SrTiO_3$. The centre has orthorhombic local symmetry and has its main axes along the [110], [1$\bar{1}$0] and [001] crystallographic directions. As is well known, hole centres are liable to exhibit reorientation effects when perturbed by externally applied uniaxial stress or static electric fields. For the hole centre of concern in this paper such effects could also be observed. This is further support for the existence of the hole centre. Furthermore, from the stress experiments the elastic dipole moment, $\beta_{[001]}$, could be determined, whereas the EPR data in the presence of static electric fields yielded the electric dipole moment, μ. The hole centre is attributed to the Fe^{2+}–O^- species which probably has been produced (with 396 nm light) from Fe^{2+}–O^{2-}. It is noteworthy that the photo-reduction of V^{5+} into V^{4+}, reported previously to occur in the same sample [5, 26, 27], could be the charge compensating counterpart of the photo-production of the Fe^{2+}–O^- defect centre in $SrTiO_3$.

Acknowledgment

One of us (ThWK) thanks Professor O F Schirmer for stimulating discussions.

References

[1] Lagendijk A, Glasbeek M and van Voorst J D W 1973 *Chem. Phys. Lett.* 20 92
[2] Lagendijk A 1974 *PhD Thesis* University of Amsterdam
[3] Schirmer O F, Berlinger W and Müller K A 1976 *Solid State Commun.* 18 1505
[4] Känzig W 1973 *J. Phys. Chem. Solids* 23 479
[5] Kool Th W 1991 *PhD Thesis* University of Amsterdam
[6] Kool Th W and Glasbeek M 1979 *Solid State Commun.* 32 1099
[7] Unoki H and Sakudo T 1967 *J. Phys. Soc. Japan* 23 546
[8] von Waldkirch Th, Müller K A and Berlinger W 1972 *Phys. Rev.* B 5 4324

[9] Blazey K W, Schirmer O F, Berlinger W and Müller K A 1975 *Solid State Commun.* **16** 1289
[10] Müller K A, von Waldkirch Th and Berlinger W 1971 *Solid State Commun.* **9** 1097
[11] Müller K A 1981 *J. Physique* **42** 551
[12] Kool Th W and Glasbeek M 1977 *Solid State Commun.* **22** 193
[13] Berney R L and Cowan D L 1981 *Phys. Rev.* B **23** 37
[14] Megaw H D 1973 *Crystal Structures: A Working Approach* (London: W B Saunders)
[15] Schirmer O F 1968 *J. Phys. Chem. Solids* **29** 1407
[16] Ikenberry D, Jette A N and Das T P 1970 *Phys. Rev.* B **1** 2785
[17] Schirmer O F 1973 *J. Phys. C: Solid State Phys.* **6** 300
[18] Possenriede E, Schirmer O F, Albers J and Godefroy G 1990 *Ferroelectrics* **107** 313
[19] Henderson B 1976 *J. Phys. C: Solid State Phys.* **9** L579
[20] Mims W B 1976 *The Linear Electric Field Effect in Paramagnetic Resonance* (Oxford: Clarendon)
[21] Kool Th W and Glasbeek M 1991 *J. Phys.: Condens. Matter* **3** 9747
[22] Itschner D 1965 *Promotionsarbeit* Eidgenössischen Technischen Hochschule Zürich
[23] Nowick A S and Heller W R 1963 *Adv. Phys.* **12** 251
[24] Landau L D and Lifshitz E M 1975 *Theory of Elasticity* (Oxford: Pergamon) p 12
[25] Schoemaker D and Lagendijk A 1977 *Phys. Rev.* B **15** 115
[26] Blazey K W and Weibel H 1984 *J. Phys. Chem. Solids* **45** 917
[27] Müller K A, Aguilar M, Berlinger W and Blazey K W 1990 *J. Phys.: Condens. Matter* **2** 2735